The Effect of Environment and Material Chemistry on Single-Effects Creep Testing of Austenitic Stainless Steels

L.B. O'Brien and B.D. Miller

Abstract Injected vacancy, enhanced creep is hypothesized to reduce crack growth rates (CGRs) in deaerated pressurized water (DPW) in austenitic stainless steels with high sulfur levels. CGR reduction is hypothesized to occur by corrosion generated vacancy/dislocation interactions that promote dislocation climb and disrupt planar slip bands. Creep tests using tensile specimens of varying sulfur content were performed in air and DPW at 288 °C. Testing began with a hold at the flow stress, followed by fatigue cycles at room temperature (RT), then holds at flow stress and 105% flow stress. Primary creep was exhibited in the high sulfur material in DPW, after the RT fatigue cycles, and resulted in 0.19 mm of extension. Characterization revealed a corrosion product and a deformed microstructure with extensive planar slip bands in the specimen that crept. Corrosion-generated vacancies are unlikely to be the source of the primary creep. Potential mechanisms for the observed creep behavior will be discussed.

Keywords Creep · 304 stainless steel · Sulfur · Hydrogen

Introduction

Corrosion fatigue crack growth rate (FCGR) testing of austenitic stainless steels (SS) in deaerated pressurized water (DPW) have shown cases of full environmental enhancement and of retardation of crack growth rates when compared to rates in air [1]. Consistent dependences of crack growth rates on test conditions and material

L.B. O'Brien (✉)
Bechtel Marine Propulsion Corporation, PO Box 1072,
Schenectady, NY 12301-1072, USA
e-mail: Lindsay.Obrien@unnpp.gov

B.D. Miller
Bechtel Marine Propulsion Corporation, PO Box 79,
West Mifflin, PA 15122-0079, USA
e-mail: Bryan.Miller@unnpp.gov

J.H. Jackson et al. (eds.), *Proceedings of the 18th International Conference on Environmental Degradation of Materials in Nuclear Power Systems – Water Reactors*, The Minerals, Metals & Materials Series, https://doi.org/10.1007/978-3-030-04639-2_59

chemistry are observed. Metallurgical sulfur content appears to correlate with the retardation of crack growth rates in DPW, but the processes that control both crack growth rate enhancement and crack growth rate retardation are not well understood [2]. Since crack growth rates can vary by several orders of magnitude depending on environment and material chemistry, a fundamental understanding of the corrosion and mechanical processes (assumed to be the primary driver of enhanced and retarded crack growth rates) that generate these changes in FCGRs must be developed in order to accurately predict the operating lifetime of light water reactor components made or clad with SS.

The injected-vacancy enhanced creep (IVEC) model proposed by Mills suggests that an increase in corrosion rates due to elevated levels of sulfur in heats of Type 304/304L SS results in metal vacancies being injected into the material ahead of a crack tip [1]. This vacancy flux was proposed to promote dislocation climb, which results in a lower crack driving force due to a disruption of the planar slip bands and subsequent blunting of the crack. Planar slip concentration, promoted by hydrogen uptake, may contribute to enhanced crack growth through more rapid coalescence of mobile dislocations into new crack surfaces [3]. The disruption due to creep of planar slip bands would thus impede this crack advance mechanism, conceptually leading to retardation. According to the IVEC mechanism, the reduction in driving force from the disruption of planar slip bands that takes place in the presence of elevated sulfur, and the resulting crack tip blunting, results in lower crack growth rates. The IVEC model predicts that creep will occur in high sulfur SS in DPW, but is not expected to occur in heats of material that have been shown to have fully enhanced FCGRs in DPW or air environments in any heat of stainless steel. Although the existence of creep would promote the creep portion of the IVEC theory, microscopy of dislocation structures can also be used to understand the role vacancies may play in promoting creep, why creep may occur in some heats of SS and not others, and the possible role of sulfur in promoting creep in DPW at temperatures where creep is not anticipated.

Primary creep has been reported in austenitic SS alloys during testing in air at temperatures less than 0.5 T_m (down to room temperature in some observations) and at stresses lower than yield [4–6]. This low temperature creep behavior is believed to occur due to a dislocation-based mechanism [5, 6]. At these temperatures, creep occurs in a single stage, in which the creep strain rate decreases over a short time interval, indicative of logarithmic behavior. Under constant stress, the decrease in creep strain rate occurs due to the reduction of mobile dislocations as the dislocations become trapped in sessile dislocation structures [5]. The dislocation density will not increase after the initial loading is complete, since the hold period at constant load will not generate new dislocations, and the fraction of mobile dislocations is expected to decrease over some (short) period of time as dislocations are trapped.

The most comprehensive compilation of austenitic SS creep data is captured by Vaillant et al. in [4], and includes results from [7]. Creep testing was performed on

square pillar test specimens in air and was performed using non-cold worked 316LN and annealed 304L stainless steels. Although this data was collected in air, it can be used to understand environmental effects, or the lack thereof. The drop in creep strain rates seen during testing in air between 200 and 400 °C has been cited as indirect support for the occurrence of the IVEC mechanism, in supposedly invalidating more conventional creep mechanisms [1]. The proposed IVEC mechanism is postulated to be operative in this temperature range (i.e., retardation in FCGR has been seen in this temperature range). Therefore, the decrease in air creep rates at these temperatures may not occur for certain heats of austenitic stainless steels in DPW, since creep may occur in DPW where none would be expected in a similar air test.

Similar mechanisms to IVEC have been proposed for creep behavior in environments where dissolution of the surface readily occurs [8]. This mechanism is based on a softening that occurs in the near surface of the material. The softening occurs when divacancies generated during surface corrosion interact with a pre-existing sessile dislocation structure and induce dislocation climb. Under the applied load, the subsequent softening of the near surface effectively reduces the cross-sectional area of the specimen allowing it to further elongate under an applied load.

Hydrogen has also been noted to have an effect on creep behavior in SS alloys. One particular study of creep in hydrogen charged 310S SS specimens at room temperature may indicate by which mechanism hydrogen affects creep [9]. In this study, creep specimens were cathodically charged at 55 °C to several atomic percent hydrogen. During short test times, on the order of 30 s, the creep rates in hydrogen-charged samples were lower than rates in uncharged samples. During this time, dislocation velocity is sufficiently slow that hydrogen readily forms an atmosphere at the dislocations and reduces/prevents slip. The opposite behavior was seen at long test times, where faster creep rates were measured in charged specimens. This was attributed to a decrease in the effect of obstacles to dislocation mobility, such as other dislocations and solutes.

The focus of this work is to determine if creep could be induced in smooth tensile specimens of Type 304/304L SS and thus test the validity of the IVEC mechanism and evaluate other potential mechanisms for creep behavior in a DPW environment. Hybrid creep/fatigue tests were performed in air and DPW to separate the effects of the corrosive environment on the underlying plastic deformation induced by a combination of tensile and cyclic loading. To better elucidate the mechanisms that may promote creep behavior, microstructural characterization was conducted to examine the oxide formed on the specimen surface and the deformation structures that formed during creep testing. The results of the work completed to date, and its implications on potential mechanisms promoting creep, are further discussed.

Experimental

Specimens

Tensile specimens in the longitudinal orientation were produced from forged bar stock of Type 304/304L SS in the as-received (mill annealed) condition. Before testing, reference marks were scribed on the specimen gauge length, which were measured before and after the test to confirm in-test measurements. Selected material chemistries are presented in Table 1. Heat A16830 is a high sulfur heat of SS, which has shown full environmental retardation under long rise time FCGR test conditions [2]. Heat 42322 is a low sulfur heat of SS, which has shown mild retardation at rise times greater than 5000 s [1]. Heat D2739 is a low sulfur heat of SS, which shows full environmental enhancement [2]. All of these specimens were tested in the mill annealed state, however, it was noted during baseline characterization work that Heat 42322 contained some level of pre-existing deformation that was not present in the other two heats despite having received nearly identical heat treatments during alloy processing.

Test Loading Conditions

Tests were conducted in air and DPW using the flow stress for each heat of material at 288 °C. These values, along with those for yield and ultimate tensile strength for each heat, are presented in Table 2. The flow stress is defined as the average of the yield and ultimate tensile stresses and was used to mimic stress levels expected within the cyclic plastic zone ahead of a fatigue crack tip. The engineering flow stress values used during testing are also included in Table 2 and differ slightly from true flow stress values. The stresses were maintained for all testing conditions in order to preserve consistency. The loading rate was kept relatively constant in order to provide accurate comparisons between the heats and environments. This is consistent with effects reported for loading rate and hold stress [5]. No changes were made to the load to account for reduction in cross sectional area as the specimen was elongated, due to the negligible amount of creep that occurred. The strains predicted from the creep testing loads are presented in Table 3.

Table 1 Average grain size and composition of select elements for Type 304/304L SS used in this testing program

Heat identification	Material	Average grain size (μm)	C	S	N	H	Fe
A16830	304/304L	137	0.019	0.030	0.082	0.0005	Bal.
42322	304	220	0.040	0.001	0.039	0.0006	Bal.
D2739	304/304L	90	0.019	0.001	0.06	0.0005	Bal.

All chemistries are in wt%

Table 2 Yield, ultimate, and flow stress for each heat of material, along with the corresponding test flow stress

Heat	Yield strength	Ultimate tensile strength	Flow stress	Flow stress used during creep test
42322	255.1	422.6	339.2	344.0
D2739	142.0	409.5	275.8	280.6
A16830	182.7	416.4	299.2	322.7[a]

All values are in MPa

[a]The corresponding load for flow stress used was greater than the true flow stress. The chosen value was maintained through all testing due to the very weak stress dependence of creep

Table 3 Predicted strain at the flow stress and 105% of the flow stress

	Flow stress		105% flow stress	
Heat	Stress (MPa)/corresponding load (kN)	Predicted strain (cm/cm)	Stress (MPa)/corresponding load (kN)	Predicted strain (cm/cm)
42322	344.0/10.9	0.07	361.3/11.4	0.09
D2739	280.6/8.9	0.07	294.4/9.3	0.08
A16830	322.7/10.2	0.11	338.5/10.7	0.13

The predicted strain levels were calculated from previously measured tensile test data. The strains are reported for the flow stress used during creep tests, as well as 105% of the flow stress condition.

Creep Testing in Air at 288 °C

Creep testing in air was performed at 288 °C and strains were measured directly on the specimen using a high temperature extensometer. The test procedure was developed in order to provide a more direct comparison to the crack tip plastic zone formed during a FCGR test. The following test plan was developed:

1. Each specimen was raised to the flow stress reported in Table 2, at a temperature of 288 °C. This load was held for approximately one week such that steady state behavior was reached. This step is denoted as Phase 1.
2. The test temperature was then lowered to room temperature, and 100 fatigue cycles were performed. All RT cycles were run with the conditions listed in Table 4.
3. The test temperature was returned to 288 °C, and Phase 1 was repeated (i.e. the test was held at the same load as in Phase 1, listed in Table 2, for approximately 1 week). This step is denoted as Phase 2.
4. The load was then increased by 5%. The test was again held for approximately 1 week. This step is denoted as Phase 3.

Table 4 Cycle conditions for room temperature cycles

Test parameter	Value
R (P_{min}/P_{max})	0.1
P_{max}	P_{max} for specimen (see Table 3)
Frequency	0.1 Hz
Rise time	5 s
Fall time	5 s
Cycle count	100 cycles
Temperature	Room temperature

Analyses of raw strain data do not provide much insight, as the initial strain during loading dominates the results. The initial loading is removed in order to examine the strain scale applicable to creep. Due to the multiple test phases, the initial strain was set to be the strain after constant load was reached, in order to remove the elongation that occurred during loading.

Creep Testing in DPW at 288 °C

Creep testing in DPW was performed in a similar manner to the air testing, such that the same test phases and loading conditions (including the room temperature fatigue cycles) were performed. Strain was measured externally of the autoclave with a linear variable differential transformer. Diurnal fluctuations in the instrumentation were seen in all heats of SS in DPW testing, due to the lack of temperature control in the lab; in these initial tests a reference LVDT was not included. By applying MATLAB's moving smoothing function, fluctuations within a span of 24 h were filtered to some extent. Again, initial strain during the first loading, as well as the loading after the 100 room temperature cycle phase, were removed in order to examine creep behavior.

Microstructural Characterization

Scanning Electron Microscopy (SEM), using an FEI Quanta 600 SEM, was employed to characterize the degree of surface oxide present on each specimen. Secondary electron images were acquired of both the surface oxide and a cross-section of the oxide after trenching with a FEI Nova 600 Focused Ion Beam (FIB) system. Transmission Electron Microscopy (TEM) was used to examine the dislocation structures that were produced during creep testing. A portion of the gauge section of each tensile bar was sectioned into 10 slices and electron-transparent thin-foil specimens were made from a 3-mm diameter discs taken from the center of each slice. This procedure enabled the deformation present in the center of the gauge section, $\sim$3 mm from the specimen surface, to be examined. Images of the dislocation structures were acquired using a Tecnai TF-20 TEM

operating in Bright-Field Scanning Transmission Electron Microscopy (BF-STEM) mode. In the foils generated from each tensile specimens, the dislocation structures were examined in 25–30 grains. Prior to imaging the dislocation structures, the thin-foil specimens were tilted to obtain two-beam bright-field diffraction contrast imaging conditions using a low order reflection.

Results

Creep Testing in Air at 288 °C

The raw strain data for all specimens is shown in Fig. 1. Figure 2 shows the creep test results with all additional strains removed for each of the three heats, i.e., those strains that were produced during changes in load (uploads and unloads), except for the final 5% upload, which was captured, as there was no unloading that occurred between the phases.

A small amount of time-dependent strain is shown in Fig. 2 during air testing. Most notably, there is a linear increase in strain seen during the first week of testing in the high sulfur specimen. In the low sulfur Heat D2739, a miniscule amount of time-dependent strain is also evident, though it is not steady state. During the

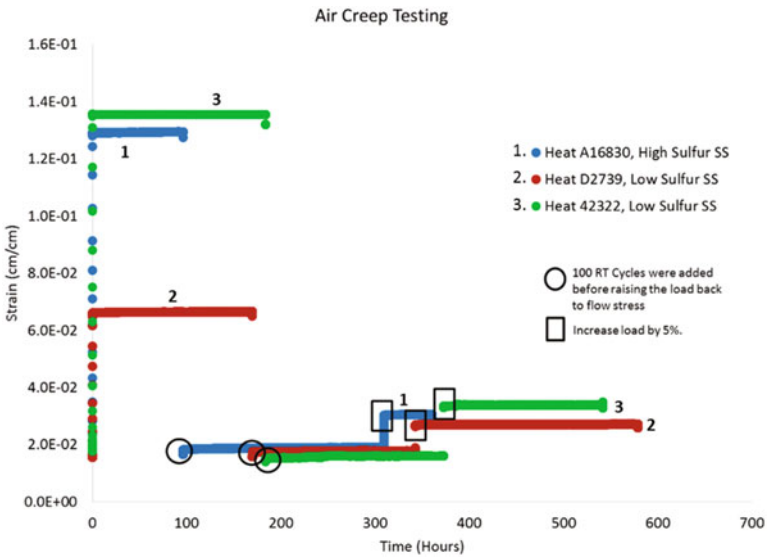

Fig. 1 Raw strain measurements for creep testing in air at 288 °C. Circles denote when the Phase 1 was completed, 100 RT cycles were added, and Phase 2 began. Rectangles denote the increase in load to 105% of the flow stress. The extensometer was removed between Phases 1 and 2, in order to perform fatigue cycles, and was therefore reset in between the phases, resulting in the apparent decrease in strain

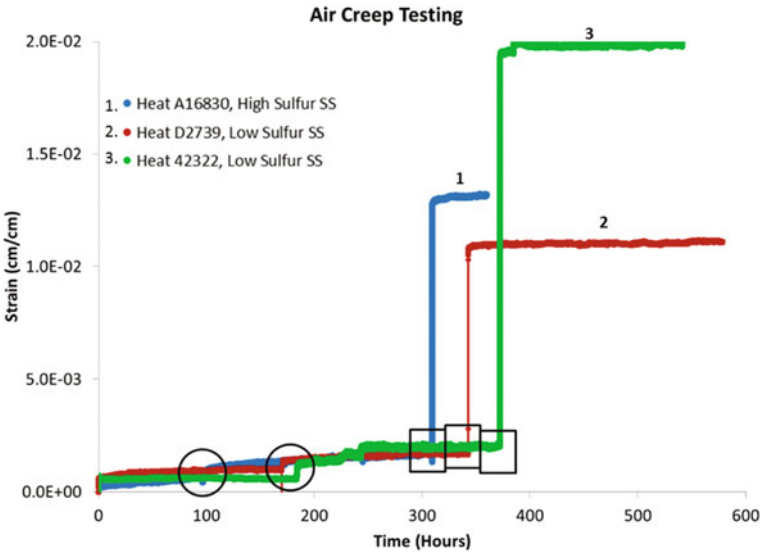

Fig. 2 Strains produced in all specimens during creep testing in air

second phase (after the room temperature cycles), all specimens show some amount of transient behavior when loaded again to flow stress. Heat A16830 appears to show the greatest amount of strain, shown in Fig. 2 between the farthest left circle and the farthest left rectangle, which donate the RT cycles and the 5% upload, respectively. Heat 42322 appears to undergo several instantaneous bursts of strain, with intervals of constant strain throughout. Finally, no significant creep strain is seen beyond the initial loading during the 5% upload portion of the test.

Creep Testing in DPW at 288 °C

The creep testing in DPW, specifically in the Heat A16830 material, was the only instance of significant creep that was measured. The filtered data without initial strains from loading is shown in Fig. 3. Two key observations can be made from Fig. 3. First, the high sulfur heat, Heat A16830, shows signs of primary creep following application of the 100 room temperature cycles. The extent of this creep is significant compared to the other SS heats in DPW and in air. The elongation during Phase 2 of this test was 185 μm over 381 h, which is substantially higher when compared to similar air results, in which the measured elongation for any test phase on any specimen was no greater than 25.4 μm. In addition to the creep seen after the 100 room temperature cycles, a less significant amount of creep may be occurring in Phase 3, after the 5% upload, as the high sulfur heat shows a more

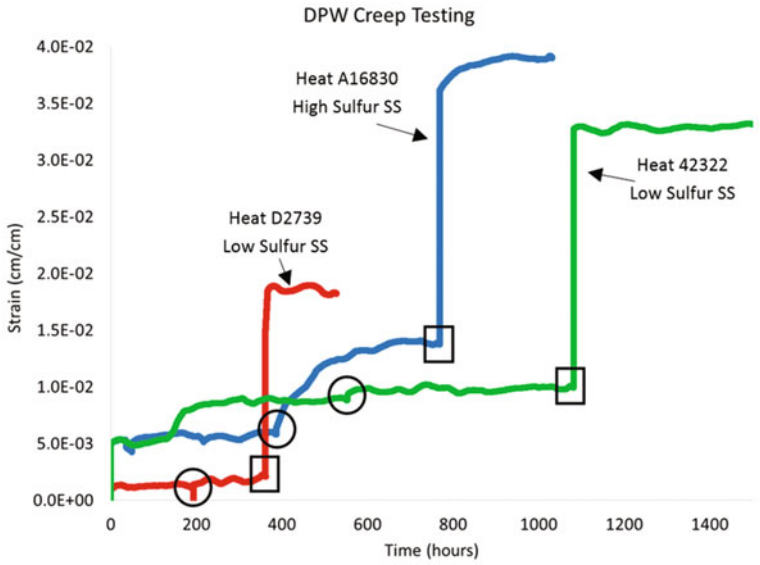

Fig. 3 Creep testing in 288 °C DPW. The high sulfur SS, Heat A16830, shown in grey, was observed to undergo creep during Phase 2, after RT cycles were performed. The arrow designates the prompt increase in strain that occurred in Heat 42322 during Phase 1

obvious increase in strain during this phase, when compared with the behavior of the low sulfur results.

The second observation regarding Fig. 3 is the prompt increase in strain that occurs in Heat 42322 during the first phase of the test. This increase is indicated by the arrow in Fig. 3, and is approximately 58.4 μm in magnitude over 37 h. The constant strain rate over a period of 37 h is indicative that this phenomenon is not a result of the diurnal fluctuations in the instrumentation, but rather a significant, measurable strain. Estimates of strain over a period of time are given in Table 5 for each specimen and each test phase in DPW. Strains measured from initial loadings are not included. The negative elongation in Phase 3 for Heat D2739 is a noise artifact, and not a true representation of elongation. The magnitude of the noise in the strain measurements in Phase 3 for Heat D2739 is approximately 6.35 μm, and for Phase 3, Heat 42322, it is on the order of 8.89 μm.

Table 5 Strain over each test phase for each heat of material

Heat	Phase 1	Phase 2	Phase 3
A16830	18.3 μm over 384 h	185.4 μm over 381 h	68.3 μm over 260 h
D2739	4.6 μm over 187 h	18.5 μm over 165 h	−6.4 μm over 153 h
42322	96.0 μm over 551 h	13.0 μm over 512 h	7.1 μm over 411 h

Microstructural Characterization of Creep Specimens

A comparison of representative BF-STEM images of the deformation structures observed in the four creep specimens from Heats A16830 and D2739 is presented in Fig. 4. Because the TEM analysis of the specimens was conducted at the conclusion of creep testing, where both tensile and fatigue loading was applied at various times, it is difficult to ascertain how each phase of testing contributed to the overall evolution of the deformed microstructure. However, some gross differences are evident between the deformation structures present between the different heats of material. In Fig. 4a, c, planar slip is observed in Heat A16830, after testing in both DPW and air, while tangles of dislocations, indicative of the interaction of dislocations on several slip planes are more prevalent in Heat D2739 after testing in both DPW and air, Fig. 4b, d, respectively. The extent of planar slip observed in

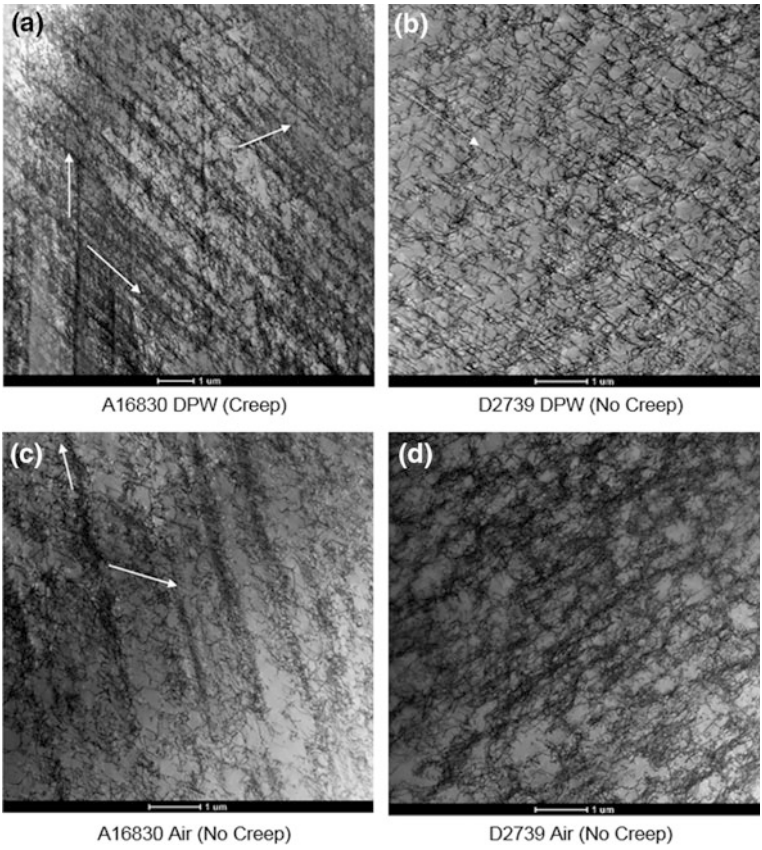

Fig. 4 Representative BF-STEM images showing the dislocation structures of four specimens. Heat A16830, shown on the left, shows clear planar slip in both air and DPW. Heat D2739, shown on the right, also shows planar slip occurring both environments

Heat A16830 is greater in the specimen that crept and is typically present on multiple slip systems. Stacking-fault ribbons, indicative of high local stresses, were also observed in higher magnification images of the planar slip bands in the specimen that underwent creep.

In addition to the TEM examinations that were performed, the surface oxides that formed on the tensile specimens were examined using SEM. Specimens from both heats tested in DPW show more extensive amounts of surface oxide relative to those tested in air. However, Heat A16830 tested in DPW exhibits a much more extensive surface oxide coverage than D2739. Cross sections through the surface oxide layer were obtained using FIB and are shown in Fig. 5. A two-layer oxide structure is observed in the specimen exhibiting creep. In the specimen from Heat A16830 that crept, Fig. 5a, this oxide consists of discrete surface magnetite particles and a thin, continuous inner oxide film that varies between ~500 nm and 1 μm. This type of structure is consistent with those found on the oxide films present on the fracture surfaces and in the crack tip enclaves of FCGR specimens tested in DPW [2]. The inner oxide film is observed to be cracked, likely from tensile loading during Phase 3, but the cracking is not observed to extend into the metal. In contrast, the surface oxide formed on Heat D2739 in DPW is much thinner, with thicker regions forming in areas corresponding to machining grooves present on the specimen surface. In air, both high and low sulfur specimens show

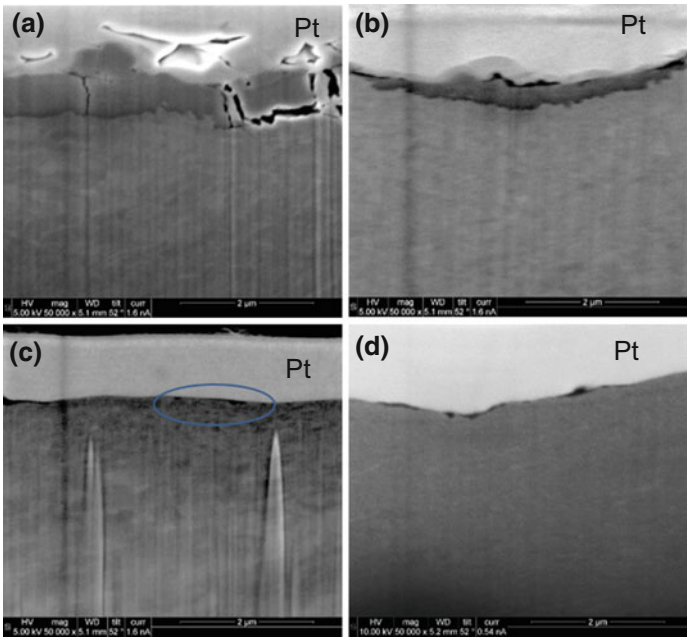

Fig. 5 Representative images of surface oxide cross sections of four specimens. Heat A16830 is shown on the left, tested in DPW (**a**) and air (**c**), and Heat D2739 is shown on the right, tested in DPW (**b**) and air (**d**). The platinum layer is identified in each image

thin oxides that form in localized regions; the degree of surface oxidation on the surfaces tested in air is substantially less than that formed in water. Finally, in all specimens, SEM imaging of the region immediately below the specimen surface exhibits features consistent with significant deformation and likely reflects damage imparted during machining of the tensile specimen.

Discussion

The results of this work suggest that creep can occur in SS having a high S content in DPW conditions at elevated temperature and is primarily observed under constant load following fatigue cycling. Further, the creep occurs over a period of nearly 400 h, which is substantially longer compared to other observations of low temperature creep reported in other SS alloys [5]. This observation suggests that the mechanism responsible for the observed creep behavior operates very slowly.

The creep rates from this work are compared to those presented in [4] in Fig. 6. For Heat A16830, Phase 2a, 2b, and 2c denote test phase 2, with "a" referring to the fastest creep rate, and "c" the slowest rate of creep. These rates were estimated by fitting portions of the curve produced during Phase 2. The minor changes in applied load between the testing environments did not result in large changes in predicted rate, confirming the results in [5].

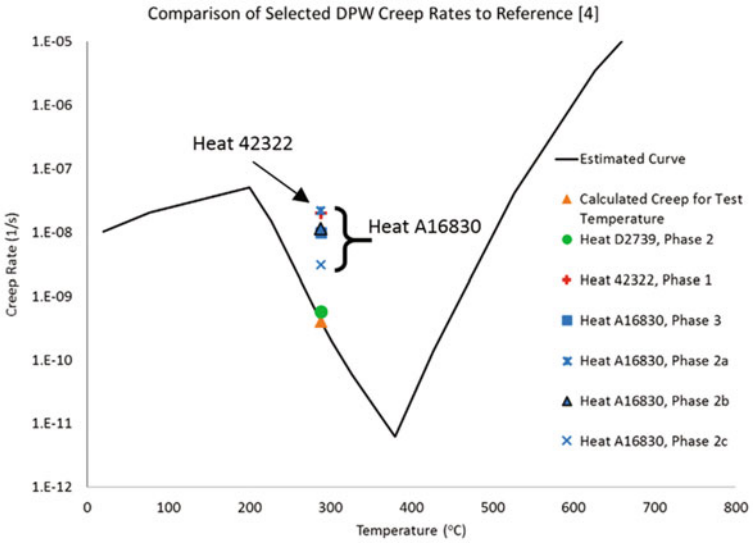

Fig. 6 Comparison of results obtained during this testing with data presented in [4]. Estimates of creep rates observed during Phase 2 primary creep that occurred in Heat A16830 in DPW are shown in blue, and are much higher than the values reported in [4], as well as the creep rates observed in Heat D2739 under similar conditions (color figure online)

The benchmark creep rate selected for Heat D2739 matches the [4] curve, and illustrates the lack of creep that was seen in the low sulfur Heat D2739, such that a suppression in creep similar to what was seen in [4] data was observed. This material has not shown retardation under normally enhanced FCGR test conditions. Heat 42322, which has shown mild retardation at long rise times during FCGR testing, was seen to have two contrasting behaviors: a short (37 h) period of elongation, with steady state regions which showed no strain. The lack of creep in Heat 42322 in Phase 2 of testing, after the 100 room temperature cycles were imparted, may be evidence of a different mechanism for retardation when compared to the mechanism for Heat A16830. This requires further testing/characterization work to determine.

The presence of a thick inner oxide layer in the specimen that crept suggests that vacancy generation, and the formation of vacancies/divacancies/vacancy clusters is certainly possible although there is no direct evidence for this with the present work. Of the mechanisms cited in the Introduction, the work of Revie and Uhlig [8], would suggest that creep could be accounted for by a reduction in strain hardening near the surface of the specimen which results from a dislocation climb process. In the Reference [8] work, testing was performed on a small (100 μm) diameter wires. Given the large diameter (6350 μm) of the tensile specimens used in this work, it is not clear if a reduction in near surface strain hardening due to vacancy-based dislocation climb mechanism would provide sufficient softening to promote the observed creep behavior. Further, non-equilibrium concentrations of vacancies are known to be produced due to fatigue loading [10]. The presence of well-defined planar slip bands near the center of the specimen suggests that any vacancies formed during the cyclic loading prior to the onset of creep did not induce dislocation climb.

In contrast to the oxidation-based mechanisms for creep, the deformation structures observed in the specimen that exhibited creep, and the time over which primary creep occurs, suggest a dislocation-based mechanism, similar to that proposed in [5], could be responsible for the observed creep. A glide-based creep mechanism was used to explain the 10–1000 s primary creep that was observed in [5], but the primary creep observed in this work occurred over approximately 400 h. Thus, in the present work, the elongation that occurred while the specimen was at constant load suggests that: (1) it took a long time for the mobile dislocations to be incorporated into sessile dislocation structures or (2) dislocation sources continued to operate under a constant applied load. The former is unlikely given the loading rates during fatigue cycling. Hydrogen, either intrinsic to the metal (i.e., hydrogen that remains in the metal after processing), or due to uptake of corrosion generated hydrogen during oxidation, is one potential source that could promote dislocation source operation by lowering the stress for dislocation nucleation and slip. The suggestion that creep processes can be dependent on hydrogen is not unprecedented, as [9] reported enhanced creep in stainless steels due to a hydrogen mechanism at 55 °C. How such a mechanism would operate is described below.

Table 6 compares the hydrogen concentration measured in the gage section (i.e., the section of the tensile specimen that underwent strain) of air and DPW creep

specimens by LECO analysis. Although the LECO analysis was performed approximately 14–18 months after testing, the diffusivity of hydrogen was low enough at room temperature (approximately 10^{-16} m^2/s) in SS that loss of hydrogen is considered negligible. For reference, in untested specimens, the baseline concentration of hydrogen in Heats D2739 and A16830 was 5 wppm (±1 wppm). The results indicate that the post-test hydrogen content remained unchanged from untested material in the specimen that underwent primary creep whereas specimens that did not undergo creep showed significant reductions in intrinsic hydrogen concentration. This suggests that there was no significant increase in hydrogen concentration in the metal resulting from the surface corrosion process.

The difference in the H measurements reported in Table 6 suggests that a significant fraction of the intrinsic hydrogen present in each of the specimens that did not creep was lost during the course of the test. A key difference between the specimen that crept and the ones that did not is the thickness of the inner oxide film formed during testing. The specimen that crept had a very thick, two layer surface oxide film compared to the specimens that did not creep. Surface oxides are known to act as a barrier to hydrogen ingress; thus, it is likely that oxides would also act as a barrier that prevents hydrogen from outgassing as well. As such, in the specimens that did not creep, the combination of (1) the lack of a thick oxide barrier, and (2) higher hydrogen diffusion rates due to elevated temperature, likely contributed to the reduction in the intrinsic hydrogen concentration observed in the LECO measurements.

Increases in hydrogen content are known to reduce the stress required for dislocation nucleation and glide in stainless steel alloys [11]. Therefore, relative to the amount of deformation induced in a tensile specimen not exposed to excess hydrogen but loaded under comparable conditions, it would be expected that higher numbers of dislocations would be generated on a given slip plane in a tensile specimen containing elevated levels of hydrogen. Further, for a given grain orientation, the reduction in critical resolved shear stress for both dislocation nucleation and glide would promote more dislocation activity on slip systems with low Schmid factors (i.e., those systems in which dislocation slip would be less/not favorable in the absence of increased hydrogen). Based on this reasoning, in Type 304/304L SS, increases in hydrogen content would be expected to produce a deformed microstructure consisting of well-defined planar slip bands, composed of large numbers of individual dislocations, on a greater number of slip systems than

Table 6 Summary of LECO hydrogen analysis from the gauge section of creep specimens

Heat	Temperature (°C)/ environment	H concentration (wppm ± 1 wppm)	Specimen exhibited creep?
D2739	288 °C/air	1	No
D2739	288 °C/DPW	2	No
A16830	288 °C/air	2	No
A16830	288 °C/DPW	5	Yes
A16830/D2739	Baseline	5	NA

would be observed in the absence of hydrogen. In the present creep testing, the concentration of hydrogen following fatigue loading may be assisted by generation of additional dislocations that serve to trap hydrogen in the gauge section of the tensile bar, locally increasing the hydrogen concentration to a higher level.

For the test conducted in which primary creep behavior is observed during a constant applied load, creep is observed over a period of several hundred hours. During this process, hydrogen would promote: (1) additional nucleation and glide of dislocations at lower stresses, leading to the formation of well-defined planar slip bands, and (2) activation of additional slip systems leading to the formation of well-defined planar slip bands on multiple slip systems. This would account for the increase in creep strain measured during creep testing. The creep strain rate would diminish with time as the increase in dislocation density on individual slip planes increases. This process would eventually induce a back stress on each slip plane sufficient to shut down dislocation nucleation and halt the creep process. Thus, a hydrogen-assisted glide creep mechanism would operate until this equilibrium is reached. Further testing will be required to determine if any amount of hydrogen present in the material could affect the dislocation nucleation/slip behavior at the temperatures at which creep was observed in the present work.

Conclusions

Creep was observed in Type 304/304L SS with high sulfur (0.032 wt%) after 100 room temperature cycles were performed in DPW. The creep recorded during this phase was the only instance of primary creep conclusively measured during testing, and resulted in an elongation of 185.4 μm over 381 h. Evidence of possible creep also existed after the load on Heat A16830 was raised by 5% in DPW (Phase 3), and also during the first hold at load in Heat 42322 in DPW (Phase 1). In the latter two specimens, it is, at present, inconclusive whether the results indicate time-dependent deformation, and further duplicate testing is needed.

Extensive planar slip, on multiple slip systems, is observed during primary creep. The deformed microstructure of the specimen that exhibited creep consisted of more well-defined planar slip deformation bands than were observed in the specimens that did not creep. This observation suggests that a vacancy-based mechanism, acting in the interior of the specimen is unlikely to influence the observed creep behavior.

SEM images of the cross-section of the surface oxide showed a much thicker, two-layered oxide formed on the surface of the high sulfur tensile specimen (Heat A16830) tested in DPW, when compared to the low sulfur specimen (Heat D2739), which exhibited a much thinner, but still two-layered oxide forming on the surface. This may indicate the mechanism for the observed creep behavior occurs by either a vacancy/divacancy softening of the near surface region or by the influence of hydrogen on promoting dislocation slip.

References

1. W.J. Mills, Accelerated and retarded corrosion fatigue crack growth behavior of 304 stainless steel in an elevated temperature aqueous environment, in *16th International Conference on Environmental Degradation of Materials in Nuclear Power Systems—Water Reactors*, Asheville, NC (2013)
2. L.B. O'Brien et al., The effect of environment, chemistry, and microstructure on the corrosion fatigue behavior of austenitic stainless steel in high temperature water, in *17th International Conference on Environmental Degradation of Materials in Nuclear Power Systems—Water Reactors*, Ottawa, Ontario, Canada (2015)
3. A. Oehlert, A. Atrens, Room temperature creep of high strength steels. Acta Mater. **42**, 1493–1508 (1994)
4. F. Vaillant, L. Tribouilloy, T. Couvant, Influence of cold work on crack growth rates of stainless steels in nominal primary environment. Workshop on Cold Work/SCC, 4–8 June 2007
5. T.H. Alden, Strain hardening during low temperature creep of 304 stainless steel. Acta Mater. **35**, 2621–2626 (1987)
6. M.E. Kassner, K. Smith, Low temperature creep plasticity. J. Mater. Res. Technol. **3**, 280–288 (2014)
7. S. Usami, T. Mori, Creep deformation of austenitic steels at medium and low temperatures. Cryogenics **40**, 117–126 (2000)
8. Revie and Uhlig, Effect of applied potential and surface dissolution on the creep behavior of copper. Acta Metall. **22**, 619–627 (1974)
9. C.W. Tien, C.J. Altstetter, Hydrogen-enhanced plasticity of 310S stainless steel. Mater. Chem. Phys. **35**, 58–63 (1993)
10. K.A. Nibur, D.F. Bahr, B.P. Somerday, Hydrogen effects on dislocation activity in austenitic stainless steels. Acta Mater. **54**, 2677–2684 (2006)
11. M. Hatano, M. Fujinami, K. Arai, H. Fujii, M. Nagumo, Hydrogen embrittlement of austenitic stainless steels revealed by deformation microstructures and strain-induced creation of vacancies. Acta Mater. **67**, 342–353 (2014)